Gaseous Protonated Nitrosyl Fluoride. Experimental and Theoretical Characterization of Two Distinguishable Isomers, HONF$^+$ and ONFH$^+$, and Evaluation of the Barrier for Their Interconversion

Massimiliano Aschi,† Fulvio Cacace,† Felice Grandinetti,*,‡ and Federico Pepi†

Università La Sapienza, P.le Aldo Moro, 5, 00185 Rome, Italy, and Università della Tuscia, V.S.C. De Lellis, 01100 Viterbo, Italy

Received: July 30, 1993; In Final Form: January 3, 1994•

The structure, stability, interconversion, and unimolecular decomposition processes of gaseous protonated nitrosyl fluoride, ONF, have been investigated by mass-analyzed ion kinetic energy (MIKE) and collisionally activated dissociation (CAD) mass spectrometry, as well as ab initio GAUSSIAN-1 calculations. Positive evidence has been obtained for the existence of two distinct, not easily interconvertible isomers, HO-NF$^+$, **1**, and ON–FH$^+$, **3**. These two species are distinguishable by both CAD and MIKE spectrometry, whose results are consistent with the theoretical description of the system. The fluorine-protonated isomer **3** is the global minimum on the surface and is more stable than the oxygen-protonated isomer **1** by 70.1 kcal mol^{-1}. Whereas isomer **3** has a low-energy dissociation channel to produce NO$^+$ and HF, the less stable isomer **1** is trapped in a deep potential well, which prevents both rapid dissociation and isomerization to **3**. The GAUSSIAN-1 potential energy diagram explains the distinctly different shapes of the MIKE peaks and the kinetic energy releases (KERs) associated with the reaction (ONF)H$^+$ → NO$^+$ + HF. The loss of HF from **3** gives rise to a narrow peak with a small KER, while the same reaction from **1** is associated with a dish-topped peak and an exceptionally large KER ($E_{t1/2}$ = 2.68 eV).

The structure, bonding, and properties of nitrosyl fluoride, ONF, are the focus of sustained interest,[1-8] recently extended to its protonated isomers whose structure and stability have been investigated at the SCF double-ζ (DZ) and SCF and CISD + Q double-ζ plus polarization (DZ + P) levels of theory.[9]

We report here a joint mass spectrometric and ab initio study of (ONF)H$^+$ ions, aimed at the first experimental characterization of the different isomers, and an evaluation of their relative stability and of the energy barriers for their interconversion.

Experimental Section

Materials. Nitrogen fluoride and nitric oxide from Matheson Ltd. and helium from Sol Sud Co. were high-purity research-grade gases used without further purification. Gaseous HF has been obtained from the thermal decomposition (t = 350 °C) of solid potassium hydrogen fluoride, KHF_2 (Aldrich Chemicals Co.) introduced into the source via the direct-insertion probe.

Mass Spectrometric Measurements. MIKE and CAD spectra were recorded using a VG Micromass ZAB-2F instrument of reversed geometry.[10] Typical operating conditions of the CI source were as follows: bulk gas pressure 0.1–0.2 Torr; source temperature 180 °C; emission current 1 mA; repeller voltage 0 V; electron energy 100 eV. The MIKE spectra were recorded using an acceleration potential of 8 kV at an energy resolution ranging from 3 × 10^3 to 6 × 10^3, and represent the average of at least 40 scans. CAD spectra were taken by admitting He into the collision cell at such a pressure to reduce the main beam intensity to 80% of its initial value. The ICR experiments were performed with a Bruker Spectrospin APEX 47e spectrometer equipped with an external ion source.

Computational Details. Ab initio quantum-mechanical calculations were performed using a RISC/6000 version of the GAUSSIAN 92 program package.[11] The standard internal 6-31G*,[12a] 6-311G**,[12b] 6-311+G**,[12c] and 6-311G**(2df)[12c] basis sets were employed throughout. Geometry optimizations were performed in the full space of the coordinates by analytical gradient-based techniques[13] in the framework of the second-order Møller–Plesset (MP2) perturbation theory,[14] employing the 6-31G* basis set. The MP2 theory was used with full electron correlation, including inner-shell electrons. The geometries obtained in this way are denoted as MP2(FULL)/6-31G*. The MP2(FULL)/6-31G* vibrational frequencies were computed for all of the investigated species, in order to characterize them as true minima, transition structures, or higher-order saddle points on the corresponding potential energy hypersurface. The unscaled values obtained were used to calculate the zero-point energies (ZPEs) of the various species. Single-point calculations, at the post-SCF level of theory, were performed within the Møller–Plesset framework up to the fourth-order (MP4), by including single, double, triple, and quadruple excitations. A post-MP4 correction for residual correlation energy contributions was accounted for by quadratic configuration interaction, including triple excitations (QCISD(T)). The GAUSSIAN-1 procedure[15] was employed to obtain the total energies of the various species and the enthalpy change of the investigated processes. This method is generally accepted as a computational procedure which is able to predict or to reproduce thermochemical data to a target accuracy of ±2 kcal mol^{-1}. The performance of this theory in the investigation of gas-phase ionic processes has recently been reviewed and its suitability amply demonstrated.[16] In the framework of the GAUSSIAN-1 approach, the total energy of a species, E(G-1), is given by

$$E(\text{G-1}) = E_0 + \Delta E(+) + \Delta E(\text{2df}) + \Delta E(\text{QCI}) + \Delta E(\text{HLC}) + \Delta E(\text{ZPE})$$

The various correction terms to the MP4(SDTQ)/6-311G** //MP2(FULL)/6-31G* total energy, E_0, are computed as follows: (i) Correction for the inclusion of diffuse sp basis functions:

$$\Delta E(+) = \text{E(MP4(SDTQ)/6-311+G**//MP2(FULL)/6-31G*)} - E_0$$

† Università La Sapienza.
‡ Università della Tuscia.
• Abstract published in *Advance ACS Abstracts*, February 1, 1994.

0022-3654/94/2098-2713$04.50/0

(ii) Correction for the inclusion of higher polarization functions on non-hydrogen atoms:

$$\Delta E(2df) = E(MP4(SDTQ)/6\text{-}311G^{**}(2df)//MP2(FULL)/631G^{*}) - E_0$$

(iii) Correction for residual correlation effects:

$$\Delta E(QCI) = E(QCISD(T)/6\text{-}311G^{**}//MP2(FULL)/6\text{-}31G^{*}) - E_0$$

(iv) Higher-level correction:

$$\Delta E(HLC) = -0.19n_\alpha - 5.95n_\beta$$

where n_α and n_β are the number of α and β valence electrons, respectively;

$$\Delta E(ZPE) = MP2(FULL)/6\text{-}31G^{*}$$

zero-point correction.

Mass Spectrometric Results

Routes to $(ONF)H^+$ Ions. Two different approaches have been successfully employed for the preparation of gaseous $(ONF)H^+$ ions under chemical ionization (CI) conditions. The first one is based on the reaction sequence

$$NF_3 + e \rightarrow NF_2^+ + F^\cdot + 2e \quad (1a)$$

$$NF_2^+ + H_2O \rightarrow (NF_2\text{–}OH_2)^+ \quad (1b)$$

$$(NF_2\text{–}OH_2)^+ \rightarrow (HONF)^+ + HF \quad (1c)$$

Using D_2O, the reaction sequence (1a–c) eventually yields labeled ions that incorporate a D atom. The reaction sequence is supported by the following observations: (i) ionization of NF_3 yields the NF_2^+ ion (m/z = 52) as the most abundant fragment, together with a minor NF^+ peak (m/z = 33). (ii) The $(NF_2\text{–}OH_2)^+$ adduct, m/z = 70, which shifts to m/z = 72 using D_2O, from the exothermic reaction (1b) is readily formed upon ionization of a NF_3/H_2O mixture. (iii) This ion undergoes loss of HF as the only metastable decomposition, thus providing evidence for the occurrence of reaction (1c). The considerable kinetic energy release (KER) of dissociation (1c), measured at the half-height of the metastable peak ($E_{t1/2}$) as 1.36 eV, suggests that a proportionately large amount of energy is deposited into the internal degrees of freedom of the $(HONF)^+$ fragment, in keeping with its tendency to undergo further metastable decomposition (vide infra). The details of the gas-phase ion chemistry of $(NF_2\text{–}OH_2)^+$ ions, in connection with the study of the protonated isomers of NF_2OH, have been reported in a separate article.[17]

Additional evidence for the reaction sequence (1a–c) has been obtained by ICR spectrometry. NF_2^+ ions have been formed by electron impact ionization of NF_3 in the resonance cell of an ICR spectrometer, isolated by multiple resonance and allowed to react with H_2O. The dependence of the abundances of all the ionic intermediates involved upon the reaction time is depicted in Figure 1. Due to the low-pressure regime of the ICR cell (P = 5.0 × 10^{-8} Torr), the $(NF_2\text{–}OH_2)^+$ ions from (1b), excited by the exothermicity of their formation process, cannot be stabilized by unreactive collisions and immediately dissociate into $HONF^+$. Moreover, in the absence of collisional stabilization, only a small but well measurable fraction of the $(HONF)^+$ ions from (1c) survives further dissociation into NO^+ and HF. From Figure 1, an additional sink of the $HONF^+$ ions is proton transfer to H_2O. As evidenced from independent double-resonance experiments, this exothermic process (vide infra) is the exclusive source of the H_3O^+ signal.

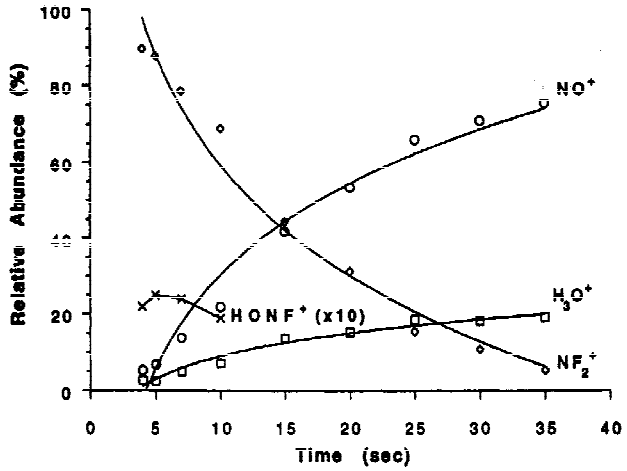

Figure 1. Time dependence of ion abundances following ionization of a NF_3 (p = 2.7 × 10^{-8} Torr) and H_2O (p = 1.0 × 10^{-8} Torr) mixture and isolation of NF_2^+.

An alternative route to gaseous $(ONF)H^+$ ions has been found in the addition

$$HF + NO^+ \rightarrow (ONFH)^+ \quad (2)$$

which occurs in a NO/HF mixture under typical CI conditions.

Structural Study of the $(ONF)H^+$ Ions. In principle, several different connectivities can be conceived for the $(ONF)H^+$ ions from reactions (1a–c) and (2), corresponding to various isomers of protonated ONF:

$$\underset{1}{HO\text{–}NF^+} \qquad \underset{2}{O\text{–}NH\text{–}F^+} \qquad \underset{3}{ON\text{–}FH^+}$$

These promoters can be discriminated by structurally diagnostic mass spectrometric techniques, and to this end mass-analyzed ion kinetic energy (MIKE) and collisionally activated dissociation (CAD) mass spectrometry have been used to detect possible structural differences among the populations of the $(ONF)H^+$ ions from (1a–c) and (2).

Irrespective of their formation process, and in keeping with the results of the ICR experiments, the only metastable decomposition of the $(ONF)H^+$ ions is the loss of HF (DF from the ions obtained from sequence (1a–c) using D_2O). This observation is consistent with the fact that elimination of HF (DF) is the energetically most favored reaction channel. However, the shapes of the peak of the MIKE spectra, shown in Figure 2, and the corresponding KER values reveal a dramatic difference between the $(ONF)H^+$ populations from reactions (1a–c) and (2). The $(ONF)H^+$ ions from reaction sequence (1a–c) show a composite, dish-topped peak (Figure 2A) with an exceptionally large $E_{t1/2}$, 2.68 eV (2.70 eV using D_2O) and a narrow central component. On the other hand, only this central component is observed in the MIKE spectrum of the $(ONF)H^+$ ions from (2) (Figure 2B). The measurement of the kinetic energy release associated to this peak is prevented by its low intensity. The observed difference in the MIKE spectra of the two $(ONF)H^+$ ionic populations is particularly telling. In fact, large kinetic energy releases and dish-topped peak shapes are generally indicative of high reverse activation energies, typical of those fragmentation processes that require prior rearrangement of the decomposing ions, whereas dissociations involving direct bond cleavage have little or no reverse activation energies and often give rise to Gaussian-type peaks.[18,19]

As preliminary noted,[20] the unimolecular decomposition of the $(ONF)H^+$ ions from the reaction sequence (1a–c) is an extraordinarily violent molecular dissociation, whose kinetic

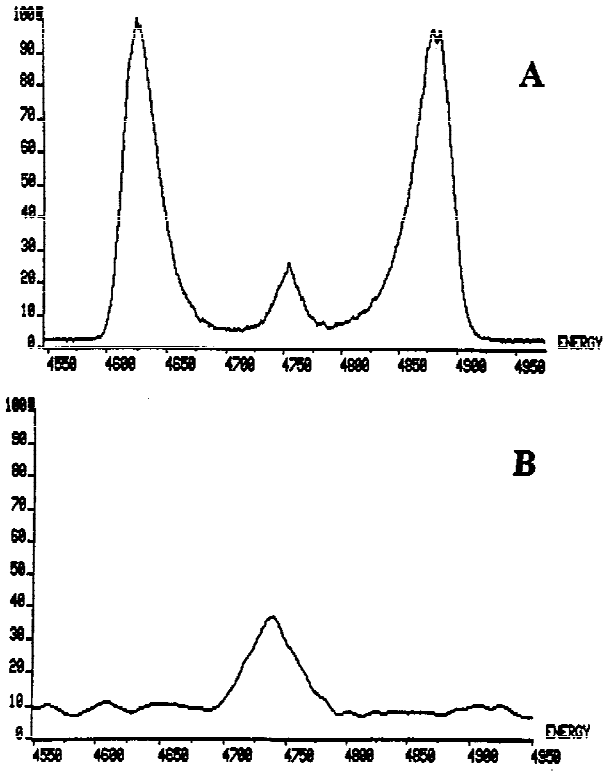

Figure 2. MIKE peaks for the decomposition $(ONF)H^+ \rightarrow NO^+ + HF$: (A) from reaction sequence (1a–c); (B) from reaction 2.

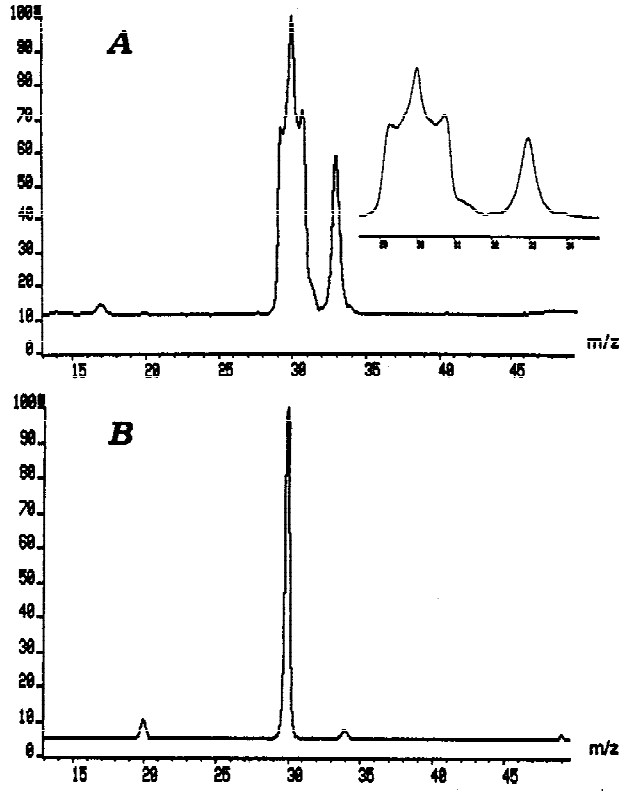

Figure 3. CAD spectra of the $(ONF)H^+$ ions: (A) from reaction sequence (1a–c); (B) from reaction (2).

energy release is unprecedented in the metastable fragmentation of singly charged cations.

Formation of different isomers has been also investigated by CAD spectrometry of the $(ONF)H^+$ populations from reactions (1a–c) and (2), although the relatively low intensity of the $(ONF)H^+$ ions and the significant contribution from their unimolecular decomposition adversely affect the quality of the CAD spectra. Anyway, formation of structurally different $(ONF)H^+$ ions from reactions (1a–c) and (2) emerges clearly from the representative spectra reported in Figure 3. Although evidence of this kind is not conclusive, the fragmentation pattern of the $(ONF)H^+$ ions from reaction sequence (1a–c) (Figure 3A), showing the NF^+ ion at $m/z = 33$ and the HON^+ ion at $m/z = 31$ (which shifts to $m/z = 32$ from the $(ONF)D^+$ ion) as the most abundant fragments, together with a structurally diagnostic OH^+ fragment ($m/z = 17$), is consistent with structure **1**. By contrast, the CAD spectrum of the $(ONF)H^+$ ions from (2) (Figure 3B), showing the HF^+ and the NFH^+ fragments, at $m/z = 20$ and 34, respectively, as the most significant ones, accords much better with structure **3**.

Theoretical Results

Details of the protonation of ONF have recently been addressed by ab initio quantum mechanical calculations.[9] The question of the existence and the relative stability of the various isomers from protonation at nitrogen, oxygen, and fluorine atoms has been examined at the CISD + Q level of theory, with a double-ζ plus polarization quality basis set. Positive evidence for the existence of four $(ONF)H^+$ distinct isomers has been obtained. The fluorine-protonated form was found to be a loosely bound complex of HF and NO^+, a view supported, inter alia, by the long distance (2.421 Å) between the two groups. This species was found to be much more stable (ca. 70 kcal $mol.^{-1}$) than the three almost degenerate (within 7 kcal mol^{-1}) ions arising from protonation at oxygen and nitrogen.

Whereas the above theoretical results are adequate for predicting the relative stability of the various $(ONF)H^+$ protomers, the question of their interconversion barriers has not been addressed. Since the knowledge of these details is crucial for the discussion of the mass spectrometric results, we decided to investigate the $(ONF)H^+$ potential energy hypersurface at the GAUSSIAN-1 level of theory.[15]

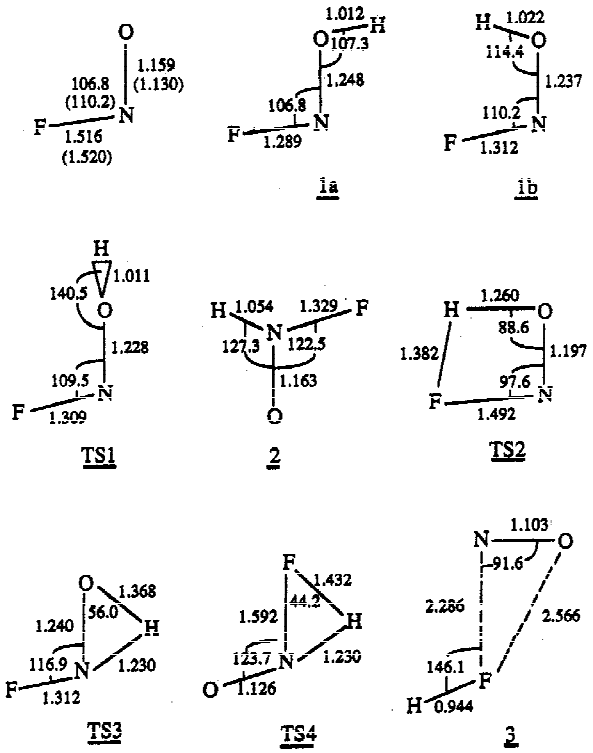

Figure 4. MP2(FULL)/6-31G* optimized geometries of the ONF molecule (experimental values in parentheses) and the $(ONF)H^+$ ions. Bond lengths in angstroms and bond angles in degrees.

Optimized geometries, at the MP2(FULL)/6-31G* level of theory, of the ONF molecule, the four $(ONF)H^+$ isomers **1–3**, and their interconnecting transition structures **TS1–TS4** are shown in Figure 4. The relevant data for the evaluation of the GAUSSIAN-1 energies of the species of interest are given in

TABLE 1: Absolute Energies (Atomic Units) of the ONF Molecule, the Investigated $(ONF)H^+$ Ions, and Their Fragments

species (NIMAG)[a]	MP2/6-31G*	MP4/6-311G**	MP4/6-311+G**	MP4/6-311G**(2df)	QCISD(T)/6-311G**
ONF (0)	−229.153 02	−229.298 49	−229.315 34	−229.416 68	−229.288 52
1a (0)	−229.344 56	−229.502 31	−229.509 65	−229.618 19	−229.496 40
1b (0)	−229.340 50	−229.496 90	−229.503 60	−229.613 77	−229.491 27
2 (0)	−229.357 41	−229.511 15	−229.518 63	−229.627 81	−229.506 86
3 (0)	−229.459 10	−229.623 93	−229.636 70	−229.726 87	−229.610 87
TS1 (1)	−229.292 65	−229.452 58	−229.460 09	−229.569 54	−229.446 80
TS2 (1)	−229.303 37	−229.456 22	−229.463 36	−229.573 20	−229.446 34
TS3 (1)	−229.262 02	−229.418 53	−229.425 85	−229.536 41	−229.406 64
TS4 (1)	−229.300 79	−229.460 62	−229.470 25	−229.577 77	−229.444 66
HF (0)	−100.184 16	−100.273 73	−100.285 82	−100.319 62	−100.273 45
NO^+ (0)	−129.248 17	−129.326 40	−129.329 49	−129.382 37	−129.313 89

[a] Number of imaginary frequencies.

TABLE 2: MP4/6-311G Absolute Energies (hartrees) and Corrections (millihartrees) for the Evaluation of the GAUSSIAN-1 Energies of the ONF Molecule, the Investigated $(ONF)H^+$ Ions, and Their Fragments**

species	MP4/6-311G**	ΔE(+)	ΔE(2df)	ΔE(QCI)	ΔE(HLC)	ΔE(ZPE)	GAUSSIAN-1	ΔE
ONF	−229.298 49	−16.85	−118.19	+9.97	−55.26	7.15	−229.471 67	
1a	−229.502 31	−7.34	−115.88	+5.91	−55.26	20.58	−229.654 30	0.0
1b	−229.496 90	−6.7	−116.87	+5.63	−55.26	20.08	−229.650 02	+2.7
2	−229.511 15	−7.48	−116.66	+4.29	−55.26	20.98	−229.665 28	−6.9
3	−229.623 93	−12.77	−102.94	+13.06	−55.26	15.83	−229.766 01	−70.1
TS1	−229.452 58	−7.51	−116.96	+5.78	−55.26	16.38	−229.610 15	+27.7
TS2	−229.456 22	−7.14	−116.98	+9.88	−55.26	14.29	−229.611 43	+26.9
TS3	−229.418 53	−7.32	−117.88	+11.89	−55.26	14.18	−229.572 92	+51.1
TS4	−229.460 62	−9.63	−117.15	+15.96	−55.26	14.63	−229.612 07	+26.5
HF	−100.273 73	−12.09	−45.89	+0.28	−24.56	9.20	−100.346 79	
								−55.5
NO^+	−129.326 40	−3.09	−55.97	+12.51	−30.70	4.83	−129.398 82	

Tables 1 and 2. The data given in Table 2 serve to discuss the energetics of the protonation of ONF, and a schematic view of the two-dimensional potential energy diagram of the relative stabilities of the various $(ONF)H^+$ species is given in Figure 5. Protonation at the oxygen atom of ONF gives stable trans and cis isomers, **1a** and **1b**, the former being more stable by 2.7 kcal mol^{-1} at the GAUSSIAN-1 level of theory. From Figure 4, and in line with previous findings,[9] comparison of the optimized structures of these protonated forms with that of ONF reveals that O-protonation shortens the F–N bond slightly but lengthens the N–O bond.

From Figure 4, and in full agreement with a previous theoretical study of neutral nitrosyl fluoride,[21] the remarkable consistency between the MP2(FULL)/6-31G* optimized parameters of ONF and the experimental data[22] has to be noted.

According to Table 2, the proton affinity (PA) at the oxygen atom of ONF, assuming the formation of **1a**, is computed at the GAUSSIAN-1 level of theory to be 114.6 kcal mol^{-1} at 0 K, which corrects to 116.1 kcal mol^{-1} at 298 K. This value is smaller than the previously reported CISD + Q energy difference between ONF and **1a**, 131 kcal mol^{-1}.[9] However, the two values are not directly comparable, since the latter does not include vibrational and thermal contributions. The interconversion of ions **1a** and **1b** occurs through the transition structure **TS1**, which lies 27.7 kcal mol^{-1} above **1a**. The single imaginary frequency of **TS1**, −1265.7 cm^{-1}, corresponds to the out-of-plane rotation of the hydrogen atom. From Figure 4, the flattening of the NOH angle (140.5°) with respect to **1a** (107.3°) and **1b** (114.4°) is noteworthy, as well as the shortening of the N–O bond distance. Consistent with the relatively high value of the computed imaginary frequency, these geometry changes indicate a significant overlap between the 2p orbitals of the adjacent N and O atoms of **TS1**.

Protonation at the nitrogen atom of ONF leads to the formation of the fully planar ion **2**, which is more stable than **1a** by 6.9 kcal mol^{-1} at the GAUSSIAN-1 level of theory. The PA of the nitrogen atom of ONF is computed as 123.0 kcal mol^{-1} at 298 K (Table 2), which is again lower than the previous CISD + Q energy difference (without vibrational and thermal contributions) of 134.6 kcal mol^{-1}.[9] As to the structure of ion **2**, our MP2(FULL)/6-31G* results are fully consistent with the previously reported CISD ones. In fact, as shown in Figure 4, protonation at the nitrogen atom of ONF results in a tighter F–N bond, whereas the N–O bond length is almost unaffected. Moreover, the increase of the FNO angle by ca. 12° as a consequence of the protonation at the nitrogen atom has to be noted. The interconversion between the O-protonated ion **1a** and the N-protonated ion **2** requires to overcome a significant activation barrier, computed at the GAUSSIAN-1 level of theory to be 51.1 kcal mol^{-1} with respect to **1a**. This 1,2-hydrogen migration process occurs through the three-center transition structure **TS3**. The single imaginary frequency associated to the ion, −1656.2 cm^{-1}, refers to the in-plane motion of the hydrogen atom, whose distances from the oxygen and nitrogen atoms are computed as 1.368 and 1.230 Å, respectively.

The ion–dipole complex **3** is obtained by protonation at the fluorine atom of ONF. As previously pointed out,[9] separation of the NO^+ and HF groups is quite large. From Figure 4, the F–N and F–O bond lengths are computed as 2.286 and 2.566 Å, respectively. From Table 2, ion **3** is by far the most stable among the various $(ONF)H^+$ protomers, e.g., it is more stable than **1a** by 70.1 kcal mol^{-1} at the GAUSSIAN-1 level of theory. Moreover, the site PA of the fluorine atom of ONF is computed to be as large as 186.2 kcal mol^{-1} at 298 K.

From the GAUSSIAN-1 energies of free HF and NO^+, reported in Table 2, the dissociation enthalpy of ion **3** into these two fragments is computed as 14.6 kcal mol^{-1}. Combining the experimental heats of formation[23] of HF, −65.1 kcal mol^{-1}, and of NO^+, 235.3 kcal mol^{-1}, with the above computed binding energy, a theoretical heat of formation of 155.6 kcal mol^{-1} is obtained for ion **3**. To evaluate the internal consistency of this value, the enthalpy change of the process

$$NF_2^+ + H_2O \rightarrow ON\text{–}FH^+ + HF \qquad (3)$$

has been calculated using the above-derived heat of formation of **3** and the experimental heats of formation of NF_2^+, 275 kcal mol^{-1}, H_2O, −57.8 kcal mol^{-1}, and HF, −65 kcal mol^{-1}. The obtained value, −126.7 kcal mol^{-1}, can be compared with the enthalpy change obtained on purely theoretical grounds. From the GAUSSIAN-1 total energies of NF_2^+, −253.585 56 au, and

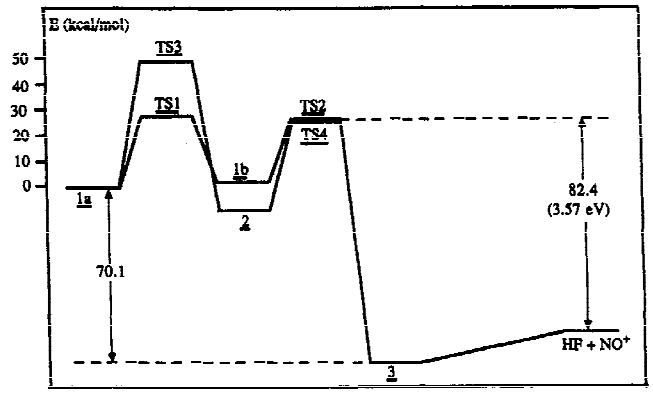

Figure 5. GAUSSIAN-1 potential energy diagram of the $(ONF)H^+$ species.

H_2O −76.327 37 au, and the data of Table 2, a value of −125.7 kcal mol^{-1} is obtained. The satisfactory agreement between the two values demonstrates the internal consistency of the computed GAUSSIAN-1 total energies.

Moreover, the GAUSSIAN-1 calculated enthalpy change for the reaction

$$NF_2^+ + H_2O \rightarrow NO^+ + 2HF \qquad (4)$$

−111.7 kcal mol^{-1}, matches the experimental value, −112.1 kcal mol^{-1}, thus providing further, independent evidence for the reliability of the computed GAUSSIAN-1 energies.

From the theoretical heat of formation of ion **3** and the previously discussed energy differences, theoretical heats of formation of 225.7 and 218.8 kcal mol^{-1} can be obtained for ions **1a** and **2**, respectively. The isomerization channels of the O-protonated and N-protonated $(ONF)H^+$ ions into the more stable ion **3** have been also investigated. Isomerization of **1a** into **3**, through ion **1b**, occurs via the four-centered transition structure **TS2**. This species, which lies 24.2 kcal mol^{-1} above **1b**, possesses a single imaginary frequency, −1843.7 cm^{-1}, associated with the in-plane motion of the hydrogen atom. From Figure 4, and consistent with the high value of the computed energy barrier, significant differences in the computed geometries of **2** and **TS2** are observed. A still larger activation barrier, 33.4 kcal mol^{-1}, is computed at the GAUSSIAN-1 level of theory for the isomerization of ion **2** into ion **3**, via the three-centers transition structure **TS4**. Also in this case, the single imaginary frequency, −1821.0 cm^{-1}, corresponds to the in-plane 1,2 migration of the hydrogen atom from nitrogen to fluorine.

Discussion

Both the mass spectrometric data and the GAUSSIAN-1 calculations point to the existence in the gas phase of two distinct, not easily interconvertible $(ONF)H^+$ isomers. A satisfactory rationalization of the experimental findings is provided by the theoretically calculated potential energy diagram depicted in Figure 5.

The CAD spectrum of the $(ONF)H^+$ ions from reaction (2) suggests that they consist of isomers of structure **3**. This finding is in keeping with their formation process, i.e., the simple addition of NO^+ to HF. In this perspective, it is legitimate to regard the ions from (2) as a model for the fluorine-protonated isomer of ONF. The ion–dipole character of this species is consistent with its MIKE spectrum. In fact, from Figure 5, it is apparent that the fragmentation of ion **3** into NO^+ and HF involves a simple bond cleavage, occurring without a significant energy barrier. As there is no reverse activation energy and the energy released from reaction (2) is small, a metastable ion peak with low KER results, as shown in Figure 2B.

A structurally different population of $(ONF)H^+$ ions is obtained from the reaction sequence (1a–c), which can be reasonably regarded as the route to the oxygen-protonated isomer of ONF, i.e., ion **1**. In fact, apart from the evidence provided from the formation process which involves the intermediacy of $(NF_2–OH_2)^+$, the H–O–N–F connectivity of the ion is consistent with its CAD and, more significantly, with its MIKE spectrum. In fact, owing to the large exothermicity of their formation process, a fraction of $HO–NF^+$ ions from (1a–c) can be formed with sufficient excess internal energy to overcome the barrier corresponding to the transition structure **TS2**, generating highly excited ions **3** that immediately dissociate into NO^+ and HF. On the contrary, extensive isomerization of $HO–NF^+$ to ion **2**, i.e., the nitrogen-protonated isomer of ONF is prevented by the significantly larger (51.1 *vs* 24.2 kcal mol^{-1}) activation barrier associated to **TS3**. From Figure 5, it is apparent that the energy difference between **TS2** and the separate NO^+ and HF fragments is large, 3.57 eV, which is reflected in the dish-topped peak shown in Figure 2A. Taking into account the evidence from the study of a large number of simple ions, the experimental $E_{t_{1/2}}$ value can be assumed to generally exceed the *mean* value of the kinetic energy release by 15–20%.[23] Under this assumption, the mean kinetic energy of the fragments would account for 60–70% of the above-computed energy difference, the remaining fraction being partitioned into their rotational and internal degrees of freedom.

The formation of the oxygen-protonated isomer of ONF from reaction sequence (1a–c) is also consistent with the results of the ICR experiments. In fact, the observed proton transfer from $HO–NF^+$ to H_2O (PA = 166.5 kcal mol^{-1}) can easily be explained in terms of the calculated proton affinity of the oxygen atom of ONF, as low as 116.1 kcal mol^{-1}. On the contrary, on the basis of the computed proton affinity of the fluorine atom of ONF, 186.2 kcal mol^{-1}, proton transfer from $ON–FH^+$ to H_2O would be predicted to be thermochemically forbidden.

Finally, the narrow component of Figure 2A, centered at m/z = 30, can be ascribed to the metastable decomposition of ions **3** formed from the isomerization of $HONF^+$ ions and stabilized by collisional deactivation in the ion source. As a plausible explanation, the isomerization can be envisaged to take place in the ion–molecule complex formed by $HONF^+$ with NF_3, whose PA, 136.9 kcal mol^{-1},[25] happens to be intermediate between the PAs of the oxygen and fluorine atoms of ONF.

Conclusions

The joint application of experimental and theoretical methods provides convincing evidence for the existence of both fluorine- and oxygen-protonated isomers of ONF as distinct species in the gas phase. The protomers are separated by significant activation barriers which prevent their facile interconversion as well as isomerization to the nitrogen-protonated isomer, whose formation was not detected in this study. The global minimum corresponds to the fluorine protonated isomer **3**, $ONFH^+$, which can be viewed as an ion–dipole complex. The oxygen-protonated form **1**, $HONF^+$, is less stable by 70.1 kcal mol^{-1}. Whereas isomer **3** has a low-energy dissociation channel to NO^+ and HF, isomer **1** is trapped in a deep potential well, which prevents both rapid isomerization and dissociation. This peculiar feature of the potential energy surface explains the different KERs associated with the dissociation of **1** and **3**, in that HF loss from $ON–FH^+$ gives rise to a narrow peak with a small $E_{t_{1/2}}$ (Figure 2B), whereas dissociation of **1** is associated with a dish-topped peak (Figure 2A) and an extraordinarily large $E_{t_{1/2}}$, 2.68 eV. CAD spectrometry has also proved useful to probe the structural differences between ions **1** and **3**, and its results are consistent with those from MIKE spectrometry, as well as with the theoretical description of the system.

Acknowledgment. Financial support by Ministero dell'Università e della Ricerca Scientifica e Tecnologica (MURST) and by Consiglio Nazionale delle Ricerche (CNR) is acknowledged.

References and Notes

(1) Schmutzler, R. *Angew. Chem., Int. Ed. Engl.* **1968**, *7*, 440.
(2) Sawodny, W.; Pulay, P. *J. Mol. Spectrosc.* **1974**, *51*, 135.
(3) Esposti, C. D.; Cazzoli, G.; Favero, P. G. *J. Mol. Spectrosc.* **1985**, *109*, 229.
(4) Pauling, L. *The Nature of Chemical Bond*; Cornell University: New York, 1960.
(5) Burkley, I. D. *Energy Res. Abtr.* **1992**, *17*, abstr. 1352.
(6) Ogai, A.; Brandon, J.; Reisler, A.; Suter, H. U.; Huber, J. R.; Von Dirke, M.; Schinke, R. *J. Chem. Phys.* **1992**, *96*, 6643.
(7) Suter, H. U.; Huber, J. R.; Von Dirke, M.; Untch, A.; Schinke, R. *J. Chem. Phys.* **1992**, *96*, 6727.
(8) Ferber, N. M.; Whitehead, J. C.; Winterbottom, F. *J. Chem. Soc., Faraday Trans.* **1990**, *86*, 1619.
(9) Meredith, C.; Davy, R. D.; Schaefer III, H. F. *J. Chem. Phys.* **1990**, *93*, 1215.
(10) Morgan, R. P.; Beynon, J. H.; Bateman, R. H.; Green, B. N. *Int. J. Mass Spectrom. Ion Processes* **1978**, *28*, 171.
(11) *Gaussian 92*, Revision A; Frisch, M. J.; Trucks, G. W.; Head-Gordon, M.; Gill, P. M. W.; Wong, M. W.; Foresman, J. B.; Johnson, B. G.; Schlegel, H. B.; Robb, M. A.; Replogle, E. S.; Gomperts, R.; Andres, J. L.; Ragavachari, K.; Binkley, J. S.; Gonzalez, C.; Matin, R. L.; Fox, D. J.; Defrees, D. J.; Baker, J.; Stewart, J. J. P.; Pople, J. A., Gaussian, Inc.: Pittsburgh, PA, 1992.
(12) (a) Hariharan, P. C.; Pople, J. A. *Chem. Phys. Lett.* **1972**, *66*, 217. (b) Krishnann, R.; Binkley, J. S.; Seeger, R.; Pople, J. A. *Ibid.* **1980**, *72*, 4244. (c) Frisch, M. J.; Pople, J. A.; Binkley, J. S. *Ibid.* **1984**, *80*, 3265.
(13) Schlegel, H. B. *J. Comput. Chem.* **1982**, *3*, 214.
(14) Møller, C.; Plesset, M. S. *Phys. Rev.* **1934**, *46*, 86.
(15) Pople, J. A.; Head-Gordon, M.; Fox, D. J.; Raghavachari, R.; Curtis, L. A. *J. Chem. Phys.* **1989**, *90*, 5622.
(16) (a) Radom, L. *Org. Mass Spectrom.* **1991**, *266*, 359. (b) Ma, N. L.; Smith, B. J.; Pople, J. A.; Radom, L. *J. Am. Chem. Soc.* **1991**, *113*, 7903. (c) Durant, R.; Rohlfing, C., *J. Chem. Phys.* **1993**, *98*, 8031.
(17) Aschi, M.; Grandinetti, F.; Pepi, F. *Int. J. Mass Spectrom. Ion Processes* **1994**, *130*, 117.
(18) Cooks, R. G.; Beynon, J. H.; Caprioli, R. M.; Lester, G. R. *Metastable Ions*; Elsevier: Amsterdam, 1973.
(19) (a) Holmes, J. L.; Terlouw, J. K. *Org. Mass Spectrom.* **1980**, *15*, 393. (b) Holmes, J. L. *Ibid.* **1985**, *20*, 1669. (c) Bowen, R. D.; Williams, D. H.; Schwarz, H. *Angew. Chem., Int. Ed. Engl.* **1979**, *18*, 451.
(20) Cacace, F.; Grandinetti, F.; Pepi, F. *Angew. Chem., Int. Ed. Engl.* **1994**, *33*, 123.
(21) Curtiss, L. A.; Maroni, V. A. *J. Phys. Chem.* **1986**, *90*, 56.
(22) Stephenson, C. V.; Jones, E. A. *J. Chem. Phys.* **1952**, *20*, 135.
(23) All thermochemical data are taken from: Lias, S. G.; Bartmess, J. E.; Liebman, J. F.; Holmes, J. L.; Levin, R. D.; Mallard, W. G. *J. Phys. Chem. Ref. Data* **1988**, *17*, Suppl. 1.
(24) Rumpf, B. A.; Derrick, P. J. *Int. J. Mass Spectrom. Ion Processes* **1988**, *82*, 239.
(25) McMahon, T. B.; Kebarle, P. *J. Am. Chem. Soc.* **1985**, *107*, 2612. (The value quoted in this reference, 140.7 kcal mol^{-1}, has been adjusted with respect to the current PA scale based on CO, cf. Szulejko, J. E.; McMahon, T. B. *J. Am. Chem. Soc.* **1993**, *115*, 7839).